Research Article Vol. 32, No. 5 / 26 Feb 2024 / Optics Express 7882
Optics EXPRESS

# Structured light enhanced machine learning for fiber bend sensing

SARA ANGELUCCI,[1] ZHAOZHONG CHEN,[1] L'UBOMÍR ŠKVARENINA,[1,2] ALASDAIR W. CLARK,[1] ADAM VALLÉS,[3] AND MARTIN P. J. LAVERY[1,*]

[1]James Watt School of Engineering, University of Glasgow, Glasgow G12 8LT, UK
[2]Department of Physics, Faculty of Electrical Engineering and Communication, Brno University of Technology, Brno 616 00, Czech Republic
[3]ICFO-Institut de Ciencies Fotoniques, The Barcelona Institute of Science and Technology, 08860,Castelldefels (Barcelona), Spain
*martin.lavery@glasgow.ac.uk

**Abstract:** The intricate optical distortions that occur when light interacts with complex media, such as few- or multi-mode optical fiber, often appear random in origin and are a fundamental source of error for communication and sensing systems. We propose the use of orbital angular momentum (OAM) feature extraction to mitigate phase-noise and allow for the use of intermodal-coupling as an effective tool for fiber sensing. OAM feature extraction is achieved by passive all-optical OAM demultiplexing, and we demonstrate fiber bend tracking with 94.1% accuracy. Conversely, an accuracy of only 14% was achieved for determining the same bend positions when using a convolutional-neural-network trained with intensity measurements of the output of the fiber. Further, OAM feature extraction used 120 times less information for training compared to intensity image based measurements. This work indicates that structured light enhanced machine learning could be used in a wide range of future sensing technologies.



## 1. Introduction

Complex optical interactions with media have captured the imagination of many researchers, becoming a rapidly growing field of cross disciplinary research [1]. When light interacts with complex media, the optical field is distorted by cascaded interactions with spatially distributed scatters or variations in refractive index [2,3]. Specifically within multi-mode fibers, manufacturing errors, bends in the fiber, and material impurities can result in distortions that lead to mode-mixing. Mode-mixing will commonly produce intricate interference between the optical modes supported by the fiber that result in output intensity profiles that resemble random behaviour rather than ordered, predictable interactions [4]. These interactions are commonly referred to as speckles, due to their complex patterning. Monitoring changes in the speckle structure has been demonstrated as a method for sensing applications [5,6]. In addition, changes in temperature and strain in the fiber lead to the intensity profile continually evolving over time, therefore it is difficult to determine explicit external environmental factors that create a particular output intensity or phase profile. This creates challenges for the use of multi-mode fibers in communications, imaging or entangled quantum systems [7].

Overcoming disorder in complex media, including but not exclusive to fiber, has led to many interesting research discoveries in communication [4,8–11], imaging [12–15], quantum optics [16–18], and optical sensors [19–24]. However, the continuous changes in relative phase between the optical modes create phase-noise that limits the accuracy of sensors based on few-mode or multi-mode fibers [24]. Intermodal coupling can be a reliable fiber property for sensing,

#513829 https://doi.org/10.1364/OE.513829
Journal © 2024 Received 8 Dec 2023; revised 30 Jan 2024; accepted 7 Feb 2024; published 20 Feb 2024

Optics EXPRESS

however a technical challenge is the development of measurement schemes that are less sensitive to changes in phase associated with thermal and mechanical effects on optical modes guided by a fiber. Low complexity, high accuracy shape sensing techniques hold significant potential for the development of fiber sensors for a wide range of novel sensing applications and would allow these sensors to be more widely deployed.

Rayleigh scattering and Bragg-grating techniques are currently the leading approach to shape sensing in fiber [25–28], where optical time domain reflectometry (OTDR) is commonly used for bend or damage location. Some bends in a fiber result in back reflections, therefore accurate measurement of the time a back reflected signal is received can reveal the location of a bend. Improvements in laser sources, interferometric techniques, and timing electronics have provided a potential road map for cm-scale bend location to be achieved. Recent demonstrations of technologies such as phase sensitive or chirped pulse OTDR, and optical frequency domain reflectometry (OFDR) have received notable interest from the community. The use of multi-mode fibers has become an emerging research avenue, with promise to increase the resolution of the bend location to around 20 m over 2 km of multi-mode optical fiber [29]. Short-distance implementations have become commercially available, with 20 cm resolution, based on multi-mode optical fiber deployed in aeroplanes and submarines [30–33]. Bragg-grating technology are use periodic grating structures are introduced into the fiber, that, when perturbed, change their period and subsequently reflect light of a specific wavelength depending on the strain or temperature change near these gratings [34–36]. Bespoke fibers have been shown to provide high accuracy shape detection, where the sensor accuracy is primarily limited by the frequency resolution of the optical spectrum analyser used for measuring frequency shifts in the back reflected signal. Although accurate, both OTDR and Bragg-grating technology are non-trivial to implement for high accuracy shape sensing, especially at *mm* scale resolution and shallow bend radii. Recent investigations have indicated that coherent detectors can be used in deployed single-mode fiber to retrieve environmental information [37]. Additionally, combinations of traditional OTDR or Bragg-grating technology with machine learning methods can improve the resolution of sensors based on few-mode fibers, but intermodal coupling and phase noise are both major limitations to accuracy of these systems [24]. Optical elements have been successfully used as all optical pre-processors for machine or deep learning to assist computational efficiency and accuracy [38–41]. Therefore, a combination of bespoke optical elements and machine learning could allow for the development of low complexity fiber shape sensors that could be transformative for consumer electronics, such as wearable technology or vehicle sensors.

In this paper, an approach which we refer to as "structured light enhanced machine learning" is demonstrated for millimeter scale bend sensing in up to a 1 km of few-mode optical fiber; an approach that specifically uses intermodal coupling as a measurement technique. Modal decomposition, commonly referred to as mode sorting or mode de-multiplexing [42–44], are optical methods for determining the linear superposition of orthogonal modes that can be used to represent any structured optical field, such as the output from a bent few- or multi-mode optical fiber, see conceptual drawing in Fig. 1. These approaches, in effect, perform an all-optical feature extraction to sort complex spatial information into a discrete set of classes, similar in concept to the use of principal component analysis of large data-sets [45]. When bends occur in fiber, light is coupled into neighbouring spatial modes. This intermodal coupling will yield a distinctive power distribution at the output of the de-multiplexer that can be used to train a machine learning algorithm. Based on statistical analysis of the power distribution, we revealed a continuously varying physical trend that can be used for accurate bend location detection. This structured light enhanced machine learning approach could also be applied to other complex systems to identify physical trends that could be used for novel sensor technologies.

Optics EXPRESS

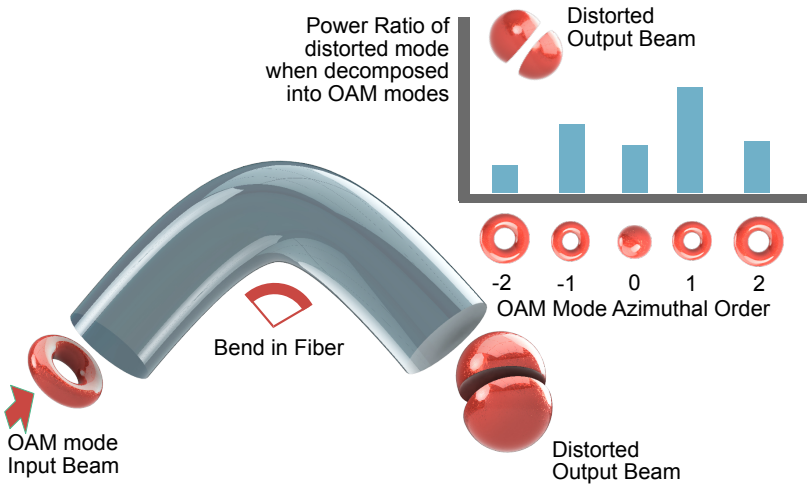


**Fig. 1.** When high order optical beams, such as those that carry OAM, are coupled in optical fibers, intermodal coupling occurs that distorts the beam. This can be measured using a mode de-multiplexer to quantify the distribution of power between OAM modes that results from intermodal coupling. When used as trainable features for machine learning, their power distributions can provide accurate information identifying the positions or degree of bending in a few- or multi-mode optical fiber.

## 2. Mode mixing in fiber

Modes in step index optical fiber are commonly considered as linear polarised (LP) modes; however, one is free to measure the light emitted from the fiber in any alternative complete modal basis. As noted above, small changes in temperature or position of the fiber usually result in chaotic changes to the relative phase noise between the modes in optical fiber, and more importantly, in a different power distribution within the supported modal bandwidth. In our experimental implementation, an orbital angular momentum (OAM) mode de-multiplexer performs an all-optical linear transformation between OAM modes and spatially separated spots on the back focal plane of a camera, [43]. This transformation is largely unaffected by relative phase, where each of the separated modes maintain their relative phase, but have only minimal levels of interference at the detector plane. Therefore, decomposing the light emitted from the fiber using an OAM de-multiplexer provides a method to monitor intermodal coupling with reduced sensitivity to undesired phase noise.

The specific mode mixing that occurs in a fiber can be represented as a transfer matrix ($\mathbf{T}$). Manufactured fibers have small variations in diameter, refractive index, mechanical twisting, and continual micro-bends along the length of the fiber. Therefore, the optical field is continually being aberrated over the full length of the fiber. This means that a transfer matrix is not valid at all length scales or positions and can be separated into distinct sections along the fiber, see Fig. 2, where each section has a ransfer matrix $\mathbf{T}_{p\pm i}$, where subscript variable $i$ indicates the sections either before or after the bend position, indicated by subscript $p$. When the position of a bend is moved, the $\mathbf{T}_p$ before the bend, $\mathbf{T}_{p-1}$, and after the bend, $\mathbf{T}_{p+1}$, will change depending on any volumetric changes in the fiber's internal structure, or the mechanical support for the fiber, and the effective $\mathbf{T}$ for the fiber as a whole will not be the same. This is mathematically represented as

$$\mathbf{T}_{p+1} \cdot \mathbf{T}_p \cdot \mathbf{T}_{p-1} \neq \mathbf{T}_{p^*+1} \cdot \mathbf{T}_{p^*} \cdot \mathbf{T}_{p^*-1}, \tag{1}$$

Optics EXPRESS

when the $\mathbf{T}$ are not an identity matrix. This can be more generally expressed for arbitrarily long fibers with $N$ segments as

$$\prod_{i=1}^{\overset{\curvearrowright}{N-1}} \mathbf{T}_i \neq \prod_{i=1}^{\overset{\curvearrowright}{N-1}} \mathbf{T}_i^*. \tag{2}$$

Therefore, as a bend position is moved, a unique distortion to the output beam profile is induced that can be used for sensing bend position. Similarly, the degree of bending will change the $\mathbf{T}_p$ for the bent region of the fiber allowing for the determination of the degree of bending. It should be noted that a straight fiber, free of micro-bend or strain would not exhibit this behaviour as $\mathbf{T}$ would not spatially change over the length of the fiber. As this behaviour requires natural variation in the fiber, a universal $\mathbf{T}$ for every fiber does not exist. Therefore, fitted, calibrated, or trained systems are required to build a sensor based on this principle.

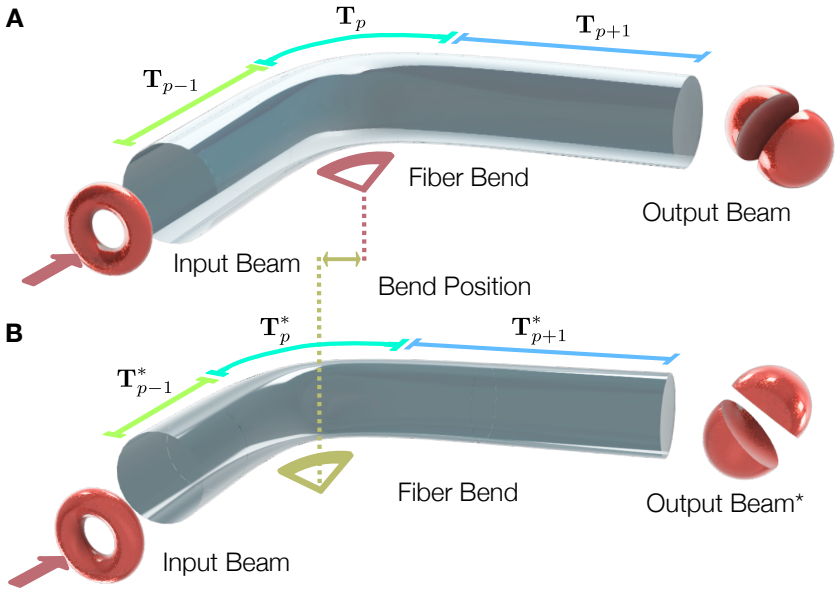


**Fig. 2.** (**A**) The transmission matrix, $\mathbf{T}$, can be separated into several sections depending on the local fiber parameters. For the case of a single bend in the fiber, with two straight sections located before and after the bend, each zone will have its own well-defined $\mathbf{T}_{p\pm i}$. In real world fiber, the straight sections will perturb the propagating optical mode. (**B**) Therefore, if the bend is moved this will lead to a change in $\mathbf{T}_{p-1}$ and $\mathbf{T}_{p+1}$, becoming $\mathbf{T}^*_{p+1}$ and $\mathbf{T}^*_{p-1}$, respectively. This will subsequently change the shape of the output beam due to different mode mixing during propagation, which can be used to determine the position of the bend.

A simplified fiber model is the matrix product of a series of $\mathbf{T}_i$ that represent the bent, $\mathbf{B}$, and straight, $\mathbf{S}_z$, regions of the fiber, where $z$ is each arbitrary longitudinal partition. To compute the expected modal distribution from the model, the straight section of the fiber is considered to have low modal mixing. This matrix is written as

$$\mathbf{S}_z = \begin{vmatrix} s_{1,1} & s^{\Delta}_{1,2} & \cdots & s^{\Delta}_{1,m} \\ s^{\Delta}_{2,1} & s_{2,2} & \cdots & s^{\Delta}_{2,m} \\ \vdots & \vdots & \ddots & \vdots \\ s^{\Delta}_{n,1} & s^{\Delta}_{n,2} & \cdots & s_{n,m} \end{vmatrix}, \tag{3}$$

Optics EXPRESS

where $s_{n,m}$ represents the power maintained in input mode when $n = m$, and $s^{\Delta}_{n,m}$ is the partial optical power coupled in neighbouring fiber modes when $n \neq m$. For the case of an ideal fiber, where no mode mixing occurs in the straight fiber $s_{n,m} = 1 \; \forall \; n = m$ and $s^{\Delta}_{n,m} = 0 \; \forall \; n \neq m$. Each column in $\mathbf{S}_z$ will sum to 1, with the assumption that no power loss occurs in this length of fiber. The bend in the fiber can be represented as a single, randomly mixed matrix, that can be written as

$$\mathbf{B} = \begin{vmatrix} b_{1,1} & b_{1,2} & \cdots & b_{1,m} \\ b_{2,1} & b_{2,2} & \cdots & b_{2,m} \\ \vdots & \vdots & \ddots & \vdots \\ b_{n,1} & b_{n,2} & \cdots & b_{n,m} \end{vmatrix}, \tag{4}$$

where $b_{n,m}$ is a random real valued number that can be described by normal distribution, as was the case for $\mathbf{S}_z$, each row in $\mathbf{B}$ will sum to 1, with the assumption that no power loss occurs at the bend. We determine the expected measured output mode as vector, $\mathbf{V}_n$. To mathematically represent a fiber with a moving bend, the fiber is segmented into 14 straight sections, $\mathbf{S}_z$, and one $\mathbf{B}$ bend location. To determine the expected output matrix, $\mathbf{V}_n$, we calculate the matrix product of all 15 $\mathbf{T}_i$. To represent the 11 bend position we considered in this work to test the principle by changing the position of $\mathbf{B}$ with respect to the other $\mathbf{T}_i$ for the same input mode. Therefore, $\mathbf{V}_n$ can be sequentially computed as

$$\begin{aligned} \mathbf{V}_1 &= \begin{vmatrix} 1 \\ 0 \\ \vdots \\ 0 \end{vmatrix} \cdot \mathbf{S}_1 \cdot \mathbf{B} \cdot \mathbf{S}_2 \cdot \mathbf{S}_3 \cdots \cdot \mathbf{S}_z, \\ \mathbf{V}_2 &= \begin{vmatrix} 1 \\ 0 \\ \vdots \\ 0 \end{vmatrix} \cdot \mathbf{S}_1 \cdot \mathbf{S}_2 \cdot \mathbf{B} \cdot \mathbf{S}_3 \cdots \cdot \mathbf{S}_z, \\ &\vdots \\ \mathbf{V}_n &= \begin{vmatrix} 1 \\ 0 \\ \vdots \\ 0 \end{vmatrix} \cdot \mathbf{S}_1 \cdot \mathbf{S}_2 \cdots \cdot \mathbf{S}_{z-1} \cdot \mathbf{B} \cdot \mathbf{S}_z. \end{aligned} \tag{5}$$

With each change in position, the effective transmission matrix of the fiber is different, yielding a change in the output modal distribution, $\mathbf{V}_n$, when $\mathbf{S}_z$ is not an identity matrix. To numerically compute the expected result, eleven effective bend positions are defined with the same real valued $\mathbf{S}_z$ and $\mathbf{B}$ transmission matrices. As each of these $\mathbf{T}_i$ will have some level of random variation, 1000 random matrices are computed for each bend, where the mean center of mass, COM, and variance is calculated. Presented in Fig. 3, is a plot of the change in average COM, $\Delta$COM, where a clear change is observed for a change in the bend position. This result indicates that for an ideal fiber, which is well supported with little or no micro-bends, no change in $\Delta$COM is calculated.

Optics EXPRESS

This result is consistent with the work by Loterie *et al.* [46]. The results indicate that increased intermodal coupling from non-ideal fiber effects result in a clear change in |ΔCOM| is expected.

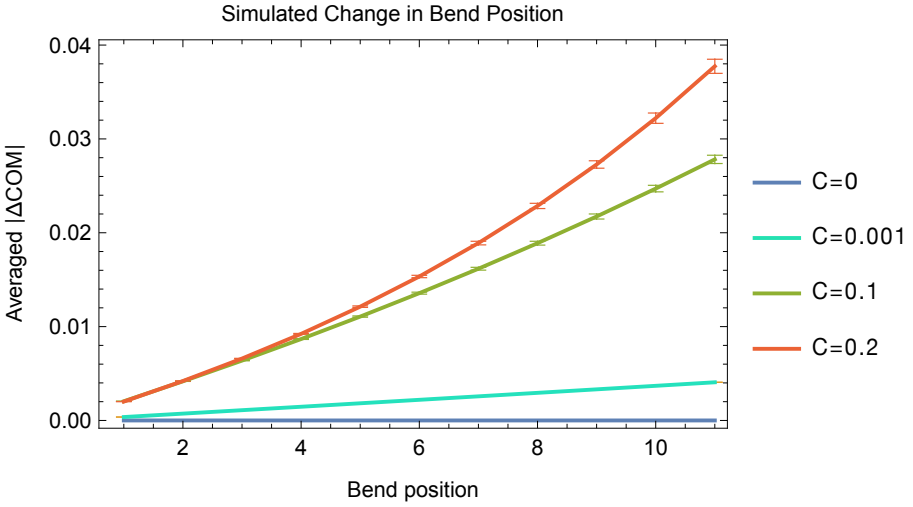


**Fig. 3.** Calculated magnitude change in center of mass, |ΔCOM| for ideal fiber with no intermodal coupling and therefore no power is transferred to any $s^{\Delta}_{n,m}$ terms in Eqn. (3) and yields $\sum s^{\Delta}_{n,m} = 0$. Intermodal coupling occurs in straight sections of fiber with small defects, therefore $\sum j_{n,m} \neq 0$. We consider a ratio, $C = (\sum_1^m \sum_1^n s^{\Delta}_{n,m})/(\sum_1^n \sum_1^m s_{n,m})$, between the total power in all $s^{\Delta}_{n,m}$ terms with relation to the total power in all $i_n$ terms, to calculate the expected |ΔCOM| in the cases where $C = \{0.001, 0.1 \text{ and } 0.2\}$, respectively.

## 3. Simulation

The spatial profile of any beam can be considered as a linear superposition of any complete basis set of spatial modes. For a coherent paraxial beam, an orthogonal set can be determined based on the particular constraints, such as Cartesian coordinates that define Hermite-Gaussian (HG), and polar coordinates that define Laguerre-Gaussian (LG) beams. Both HG and LG modes have been used to decompose optical fields from fiber [44,47], however selection of the wrong basis set could lead to additional errors due to inter-channel crosstalk [44]. LG beams are commonly used for expressing spatial modes bound by circular apertures. Linear-polarised (LP) modes, commonly considered in step index fiber, can be readily expressed as linear super-positions of $\mathrm{LG}_{p,\ell}$ modes, where spatial modes are described by two integers, $p$ and $\ell$, that correspond to radial and azimuthal components, respectively. a linear superposition can be expressed as:

$$\Psi(r,\rho) = \sum_{\eta=1}^{N_{\mathrm{B}}} \alpha_\eta \exp(i\phi_\eta) \cdot \Psi_\eta(r,\rho), \tag{6}$$

where $\eta$ is an integer assigned to a radial–azimuthal pair as $\eta = (p,\ell)$, thus $\Psi_\eta(r,\rho)$ is the complex spatial field of each $\mathrm{LG}_p^\ell$ mode supported by the optical system given by $N_{\mathrm{B}}$, $\alpha_\eta$ is the amplitude weighting of each mode, and $\phi_\eta$ is the relative phase between each mode. When intermodal coupling occurs at a bend in a fiber, power in one particular spatial mode is distributed between neighbouring spatial modes. The relative phase noise is largely affected by even small temperature changes or strain on the optical fiber. These relative phase shifts will continually vary with respect to time and environmental conditions. Therefore, it can be approximated to a random variation in time. As our modal decomposition method allows us to minimise the

Optics EXPRESS

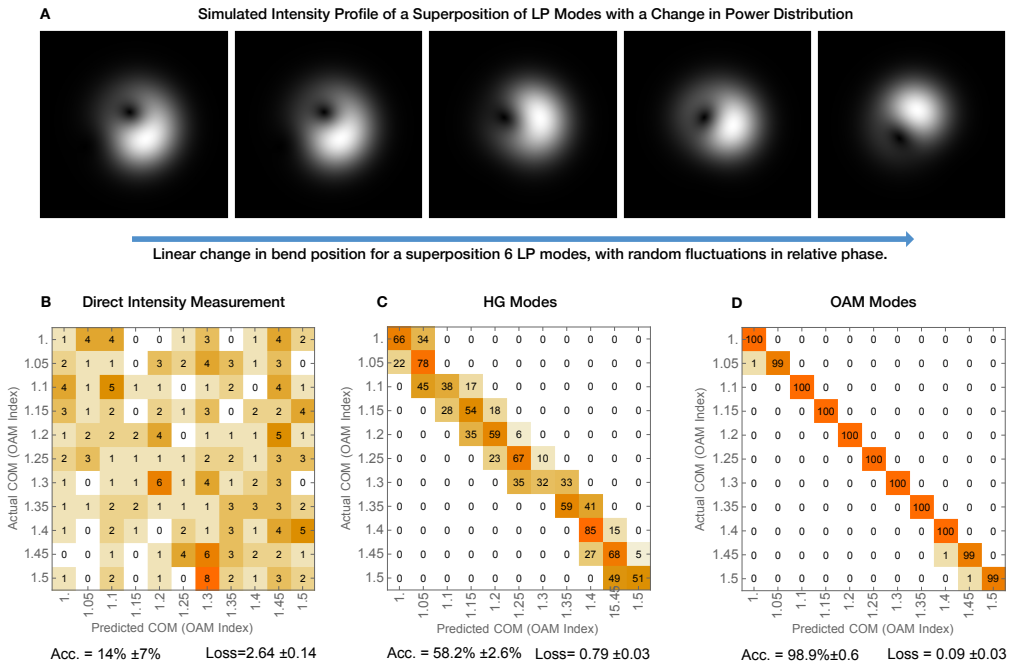


**Fig. 4.** The measurement of bend location from intermodal coupling was simulated to compare different machine learning approaches for the detection of intermodal coupling when relative phase will naturally evolve. (**A**) a series of sample intensity profiles with a change in COM, with random relative phase noise between modes used for training. (**B**) a neural network trained using direct intensity measurement of intensity is considered as the bench mark for traditional approaches using machine learning. The use of modal decomposition in both the (**C**) HG and (**D**) LG basis sets are considered, indicating OAM is the preferred basis set for accurate identification of intermodal coupling.

influence of relative phase noise on the measure of intermodal coupling, it can improve the overall accuracy of our proposed sensing technique. We note, bend or movement of the fiber that do not introduce changes in intermodal coupling and relative phase shifts only, would not be detectable in our current approach.

In our experimental implementation we utilise a step index fiber with a core size of 8.2 μm (SMF28) and couple in light from a laser of wavelength 660 nm. At this wavelength, the fiber will support multiple modes and can be considered a few-mode optical fiber. LP modes are commonly considered the orthogonal mode set of step index bounded waveguides. We estimate our fiber can support 6 spatial LP modes, where the intermodal coupling results in the output mode after bending being a linear superposition of these modes. Therefore, to replicate this intermodal coupling, 11 unique, but non-orthogonal, superpositions of LP modes were generated with random relative phases between each spatial mode.

A common approach for spatial modal analysis using machine learning is based on trained neural networks and has shown promise for communication and sensing systems [48]. Therefore, we utilise a neural network as a bench mark to compare mode structured light enhanced machine learning, see Fig. 4**B**, where we image the output of the fiber directly onto a CCD camera. Our simulated modal decomposition is achieved by computing the overlap integral of the output with HG and OAM modes, as all-optical mode sorting techniques exist for these mode types [44,49], Fig. 4**C** and **D**, respectively. These results indicate that OAM decomposition performs substantially better than either direct intensity measurement 14% or using HG modes 58.2%,

Optics EXPRESS

yielding 98.9% accuracy for the identification of intermodal coupling. We note training can also be completed using both phase and intensity information of the output optical beam from the fiber, however our simulations indicate an 11%±7 accuracy with a loss of 2.76±0.15. This lower accuracy is related to the large potential variations in phase that occur from random phase-noise, leading to additional error during training for a given training set.

## 4. Experimental implementation

Experimentally, a loosely supported fiber was bent at a series of positions and with bends of different radius of curvature, where the spatial mode decomposition into the OAM basis was recorded. Two types of fiber configurations were considered in these experiments, a laser with a wavelength of 660 nm was used in conjunction with 8.2 μm core few-mode fiber (SMF28, which is commonly used as single-mode fiber for 1550 nm) and 50 μm core step index fiber (M14L, Thorlabs). Through structured illumination and controlled coupling to the optical fiber, both fundamental and higher order LP modes could be excited. A spatial light modulator (SLM) (Cambridge Correlator SDE1024n) screen is imaged onto the back focal plane of a 10× microscope objective (Olympus RMS10x) such that the fiber facet is in the farfield of the SLM. Free-space optical to fiber coupling is controlled with a three-axis stage (Thorlabs MBT616D/M). The output of the optical fiber is then either directly imaged onto a CCD camera (Imaging Source Skyris) for the intensity retrieval results, see Fig. 5**A**, or de-multiplexed into OAM modes for further increase of the accuracy, as shown in Fig. 5**B** and **C**. We utilise a passive optical device designed for the sorting of beams that carry OAM to perform a modal decomposition of the light emanating from the fiber. This device performs a log-polar transformation, which subsequently allows a spherical lens to convert beams that carry angular momentum into a series of separated spots at the back focal plane of a lens [49]. The sorter utilised in our experiment comprised two free-form optical surfaces to perform the required transformation, where the optical profiles

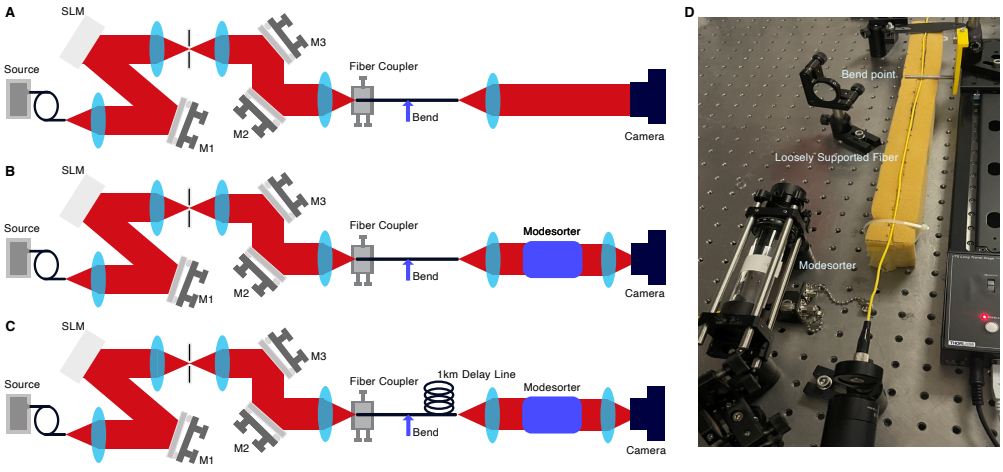


**Fig. 5.** To determine the usefulness of our modal decomposition approach we investigated three setup configurations to measure the output from the fiber. (**A**) First, the directly measured intensity of the output mode to train the CNN, for the results shown in Fig. 7**A**. (**B**) a log-polar optical transformer was used to perform OAM de-multiplexing of the output from the both few- and multi-mode optical fiber, for the results shown in Fig. 7 **B** and **C**. (**C**) To explore the use of the technology for remote sensing, a 1 km delay line of few-mode fiber was introduced. For each realisation, the fiber was bent at 11 fixed locations using a computer controlled translation stage. (**D**) a picture of the experimental setup, showing the loose support for the fiber, the mode-sorter and moving bend position.

Optics EXPRESS

for each of the surfaces are fully outlined in [50]. The surfaces used had an aperture diameter of 12.5 mm, which were directly machined on each side of a 10 cm long bar of polymethyl methacrylate (PMMA), utilising the same machining method as outlined in [50].

The bends are induced by pressing down on the fiber with a 5 mm diameter bar that is mounted with a low drag ball bearing to prevent torsion on the fiber. The fiber is supported by memory foam with a channel to prevent bending in locations other than those specifically induced, see inset of Fig. 5**D**. Although supported, the fiber will naturally change shape slightly in other positions; however, resembles real-world scenarios that would be experienced in applications such as wearable fiber sensors. This bar is mounted to a linear translation stage (Thorlabs LTs300/M) to allow for repeatable bending. The radius of curvature was altered by varying the height of the bar inducing the bend in the fiber. For the experimental simulation of remote sensing applications, we introduce 1 km of SMF-28 fiber delay line and repeat these same measurements.

## 5. Results

Each bend position and radius was recorded 100 times, to record changes in laser power or optical coupling. The process was repeated 10 times so that experimental variation in the support, temperature, and strain on the fiber were fully recorded, see Fig. 6. Selected distributions from one data set are presented in Fig. 6**A**, where a small variation in the weighting of the normalised power distribution can be observed with a change in position of the bend. A common method of analyzing power distribution of OAM is calculating the center of mass (COM), [51]. As this distribution will vary slightly over time or repeated relocation of the bend conditions, the average and standard deviation of the COM was calculated for all 1000 distributions measured for both few- and multi-mode fiber, see Fig. 6**B**.

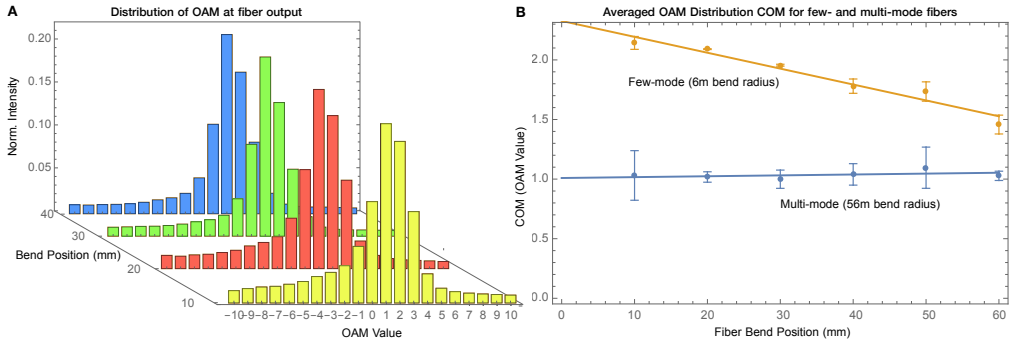


**Fig. 6.** A modal decomposition of the output of a few-mode optical fiber was measured for a range of position and radius of curvatures, utilising an all-optical log-polar transformer. The unique distribution was recorded at each position, which depended on the input mode and accumulative transfer matrix of the fiber. (**A**) When a $LG_{0,\ell=2}$ mode is coupled into the fiber and a change in bend position is made, it can be seen that there is a subtle change in power distribution. (**B**) When analyzed, on average, a continuous change in center of mass (COM) was observed in both few- (yellow curve) and multi-mode fiber (blue curve).

As the bend position is moved, the propagation length within the fiber after the bend is increased, this creates further intermodal coupling due to the change in effective transmission matrix of the straight region after the bend. As a result, the COM varies linearly when the bend is positioned further away from the receiver, as predicted in the simulations from Fig. 3. We further observe a difference in the gradient when there is a change in radius of curvature of the bend. The increased bend radius will result in increased intermodal coupling in the fiber and will accelerate coupling to other modes, see Fig. 6**B**.

Optics EXPRESS

These physical features confirm that machine learning can provide a useful tool for classifying the bend positions within the data. The experimental data was processed using a convolutional neural network (CNN) for images of the directly recorded optical field intensity, showing low accuracy in the recognition of bend locations in the fiber, see Fig. 7**A**. Given the non-standard nature of the images we wish to process from the optical fiber, we developed a simple CNN comprising five layers; a convolution layer (20 outputs and $4 \times 4$ kernel size), pooling layer, flatten layer, linear layer and softmax layer. We note, the purpose of this investigation is not to obtain the best possible accuracy CNN model, but simply to give a benchmark that we can directly compare our modal decomposition approach with the same physical parameters. Our training set comprised of data from three independent measurement data sets from the experimental system and our verification was from a fourth independently measured data-set. This approach was to ensure we do not train for random fluctuations in the fiber that occur from temperature, small mechanical changes, or fiber mounting. The memory requirement for images used in this training was approximately 5Gb, comprising 50×50 8-bit images. The computer used was an Apple M1 MacMini, with 8 CPU cores, 7 core neural engine, and 16GB of physical memory. The neural network was implemented in Mathematica, utilizing the NetTrain tools to develop our network. Training took approximately 4 hours. The 100 images connected with each position were labeled with the position and input mode only, the network was not aware of the specific measurement data set that each image was recorded within.

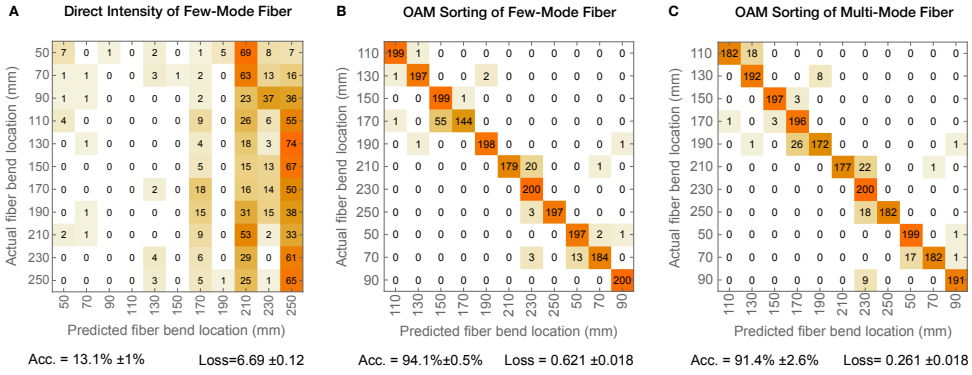


**Fig. 7.** (**A**) The output from a few-mode optical fiber was directly recorded for a range of different bend locations, indicating low accuracy in training based on a CNN. (**B**) Using the same few-mode fiber, training was completed on model de-multiplexed into the OAM modal basis showing high accuracy in bend location. (**C**). The experiment was repeated using 50 μm core step index multi-mode fiber, again showing high accuracy in bend location. For all plots, verification was completed using dedicated measurement completed later in the day.

We implemented support vector machine (SVM) training on the OAM spectrum for both few- and multi-mode fibers, showing greater accuracy in classification, up to 94.1%, as shown in Fig. 7**B** and **C**. A further advantage of this form of machine learning training is the reduction in training time required; where over 4 hours is required for image based CNN and only 3 minutes for OAM spectrum based implementations. Our verification in both cases utilises data collected from a different experimental realisation approximately 3 hours after the initial training data is recorded, therefore no data in the training set is used for verification. This confirms that the data is robust to the natural changes throughout the day. Due to the reduced processing time we could increase the number of samples to 200 samples at each position used for training to capture more variation from environmental effects. This is increase in samples lowered our accuracy by approximately 2% due to increased thermal drift. Experimental studies were conducted in an

Optics EXPRESS

environment with a temperature variation of 2-3 degrees Celsius over the length of the day. To explore the use of the technology for remote sensing, a 1 km delay line of few-mode fiber was introduced and the accuracy of bend location measured. Table 1 shows the combined results for few-mode fiber measurements for different distances and steps between the locations of the bends.

**Table 1. Accuracy results for different fiber lengths of few-mode for a measurement based on OAM sorting and trained network using SVM, similar to the results shown in Fig. 7B and C.**

| Fiber Length | 1 mm Step | 10 mm Step |
|---|---|---|
| 1 m | 86.5% | 94.1% |
| 1 km | 84.2% | 90.5% |

## 6. Discussion

Reducing the sensitivity to relative phase noise through the use of modal decomposition reveals features within the intermodal coupling that can provide accurate information about the shape or position of bends in the fiber. For convenience, our initial investigation used an SLM to excite specific modes in the fiber. However, a simpler approach to induce these same higher order modes is to illuminate the fiber using an off axis Gaussian laser [4]. Our current experimental approach, is a proof of concept bench top experiment, however physical size and complexity could be reduced through the implementation of compact mode sorters that directly attached to fiber such as those demonstrated by Lightman *et al* [53]. Our current demonstration is limited to bends in a single direction and over known fiber lengths, where future work will investigate the viability to detect multiple bends with modifications to the system training or illumination modes. We note in our current implementation, that bends in multiple directions, or over longer or shorter fiber could result in errors in classification. Retraining will be required for substantive changes in system, such as the laser source, optical coupling components or fiber type; however, once fully trained, *retraining* is not generally required for weeks to months, under normal heat cycling. Further investigation for extreme changes in temperature, such as those for aeroplanes, would be required for the development of prototype systems. For sensitivity to multiple directions, we suggest multi-core fibers could be used to measure the differential in bend state at each fiber, similar to that done with bespoke Bragg grating fibers. In addition to the reduced training complexity, an implementation advantage to using mode de-multiplexing based sensing, is it will be directly compatible with space division multiplexing systems, where sensing could be implemented along side communications without the requirement for the addition of high resolution cameras. We propose one could develop systems for fiber shape sensing in a range of applications, including movement sensors for wearable technologies, flexure hinge monitoring, or aeroplane wing shape sensing. Further investigation for extreme changes in temperature, such as those for aeroplanes, would be required for the development of prototype systems.

Previously demonstrated speckle-based sensors could potentially address the challenges of phase noise by increased complexity in machine learning approaches and using larger data sets to sample the potential variation in the speckle from non-mechanical environmental factors. We expect this would dramatically increase the required training for speckle-based approaches compared to mode-demultiplexing approaches we have presented. Our all-optical processing, using modal decomposition, optimizes the amount of information that is required to be collected when analyzing spatial information due to geometrical similarities between particular modes. For example, in order to perform a phase and intensity reconstruction of an OAM mode, we will require an array of complex values to record the profile in both phase and intensity across a system

Optics EXPRESS

aperture. The Nyquist sampling imposes a strict limit on the minimum number of spatial samples that are required to be taken to fully resolve an optical field, which requires 2 sample points per phase change of $2\pi$. Therefore, for an OAM mode with $\ell = 10$ any measurement system would require at least 20 sample points around the annulus of the beam, plus one additional pixel to identify the direction of the twisted phase front. Usually, optical information is recorded on a camera, therefore these 21 sample points mapped onto a square grid will require each side of the grid to have $d = 21\pi^{-1} \approx 7$ therefore requiring a grid of at least 49 pixels. However, when partnered with a mode-sorter, the same OAM mode can be recorded as a single complex number. When complex data is recorded as two 8-bit values for intensity and phase, 16 bits per pixel are required. Our experimental implementation utilises 21 OAM modes, and after de-multiplexing we only record intensity information, which corresponds to 8-bits per mode. Therefore, a reduction factor, $\beta$ fundamentally required information of

$$\beta = \frac{b_1 \left(\frac{2\ell_{\max}+1}{\pi}\right)^2}{b_2\,(2\ell_{\max}+1)} = \frac{b1}{b2}\frac{(2\ell_{\max}+1)}{\pi^2}, \tag{7}$$

where $\ell_{\max}$ is the maximum OAM mode, and $b_i$ is the bit depth for the recorded data in both measurements being compared. In our approach we sample 21 modes, covering the range $\ell = \pm(1, 2, \ldots, 10)$, which is oversampling modal bandwidth of the fiber. For our system, this means utilising modal decomposition compared to training in a pixel basis comprising both phase and intensity reduces the information required for training by a factor of $\beta = 4.25$. Utilizing solely intensity information, the required information results in a reduction factor of $\beta = 2.25$. However, we recorded our data with much higher resolution to reduce error from camera centering, pixel edge effects, and noise (we recorded 640 by 480 pixel images, reduced to 50 by 50 pixels for training). To confirm the optimal resolution, images were subsequently down-sampled to 5 by 5, 10 by 10, 25 by 25, and 50 by 50, resulting in a training accuracy of 6.0 ± 0.7%, 7.6 ± 0.8%, 9.5 ± 0.9% and 13.1 ± 1% respectively for a baseline accuracy of 9.1%. Our OAM sorter (that records 210 by 100 pixels on a camera, down sampled to 21 values) achieved 94.1% for the same bend spacing. Our experimental results show a 120 times reduction in the amount of training information required for training by decomposing 2D spatial information, into only 21 8-bit values. We note the reduction in training information required in our demonstration are due to the specifics of measurement approaches outlined and the geometric similarity between OAM modes and LP modes in step-index fibers. The fundamental information capacity limits of different spatial basis are discussed in detail by Zhao *et al.* [52].

In conclusion, we have developed a robust, novel fiber bend sensor that can reveal the location of bends using the intermodal coupling induced by this bend. A mode de-multiplexing approach is used to perform efficient all optical pre-processing of the observed intermodal coupling, simultaneously increase measurement accuracy, from 13% accuracy to over 80%, and reduce the training information required for the machine learning algorithms used for bend position recognition by a factor of 120. More generally, mode de-multiplexing combined with machine learning is a potentially powerful technique that could be deployed for a wide range of applications, where the constant evolution in relative phase between modes can be considered as noise within the system. These applications could include monitoring atmospheric conditions or retrieving information from dense scattering environments. Similar mode-demultiplexing approaches could be used to analyze statistical variations in relative phase to further increase system sensitivity.

**Funding.** Fundacio Cellex, Fundacio Mir-Puig, Generalitat de Catalunya through CERCA (CEX2019-000910-S); The Leverhulme Trust (RPG-2018-149); BBSRC (BB/N016734/1, BB/T000627/1); Engineering and Physical Sciences Research Council (EP/T517896/1, EP/V030515/1, EPSRC EP/T009047/1).

**Acknowledgements.** The authors would like to thank Steven Simpson for useful conversations and Lucia Uranga for proofreading services. The work was supported by the Horizon 2020 Future and Emerging Technologies Open

Optics EXPRESS

grant agreement "Super-pixels" No. 829116, the EPSRC (grant numbers EPSRC EP/T009047/1, EP/T517896/1, and EP/V030515/1), the BBSRC (grant numbers BB/T000627/1 and BB/N016734/1), The Leverhulme Trust (grant number. RPG-2018-149), Grant CEX2019-000910-S funded by MCIN /AEI/ 10.13039/ 501100011033, Fundació Cellex, Fundació Mir-Puig, Generalitat de Catalunya through CERCA.

**Disclosures.** The authors declare no conflicts of interest.

**Data availability.** Data underlying the results presented in this paper are not publicly available at this time but may be obtained from the authors upon reasonable request.

## References

1. J. Ladyman, J. Lambert, and K. Wiesner, "What is a complex system?" Eur. J. for Philos. Sci. **3**(1), 33–67 (2013).
2. A. N. Kolmogorov, "The local structure of turbulence in incompressible viscous fluid for very large Reynolds numbers," Proc. The Royal Soc. **434**(1890), 9–13 (1991).
3. S. Viola, Z. Chen, A. M. Yao, *et al.*, "Degradation of light carrying orbital angular momentum by ballistic scattering," Phys. Rev. Res. **2**(3), 033093 (2020).
4. J. Carpenter, B. J. Eggleton, and J. Schröder, "Complete spatiotemporal characterization and optical transfer matrix inversion of a 420 mode fiber," Opt. Lett. **41**(23), 5580–5583 (2016).
5. P. J. Kajenski, P.L. Fuhr, D.R. Huston, *et al.*, "Mode coupling and phase modulation in vibrating waveguides," J. Lightwave Technol. **10**(9), 1297–1301 (1992).
6. I Floris and J. M. Adam and P.A. Calderón and S. Sales, "Fiber Optic Shape Sensors: A comprehensive review," Opt. Lasers Eng. **139**, 106508 (2021).
7. H. Cao, S.-C. Gao, C. Zhang, *et al.*, "Distribution of high-dimensional orbital angular momentum entanglement over a 1 km few-mode fiber," Optica **7**(3), 232 (2020).
8. R. Ryf, N. K. Fontaine, H. Chen, *et al.*, "Mode-multiplexed transmission over conventional graded-index multimode fibers," Opt. Express **23**(1), 235–246 (2015).
9. J. Carpenter, B. J. Eggleton, and J. Schröder, "Observation of Eisenbud–Wigner–Smith states as principal modes in multimode fibre," Nat. Photonics **9**(11), 751–757 (2015).
10. B. Nenad, Y. Yang, R. Yongxiong, *et al.*, "Terabit-Scale orbital angular momentum Mode Division Multiplexing in Fibers," Science **340**(6140), 1545–1548 (2013).
11. H. Huang, G. Milione, M. P. J. Lavery, *et al.*, "Mode division multiplexing using an orbital angular momentum mode sorter and MIMO-DSP over a graded-index few-mode optical fibre," Sci. Rep. **5**(1), 14931 (2015).
12. T. Čižmár and K. Dholakia, "Exploiting multimode waveguides for pure fibre-based imaging," Nat. Commun. **3**(1), 1027 (2012).
13. A. P. Mosk, A. Lagendijk, G. Lerosey, *et al.*, "Controlling waves in space and time for imaging and focusing in complex media," Nat. Photonics **6**(5), 283–292 (2012).
14. D. Stellinga, D. B. Phillips, S. P. Peter, *et al.*, "Time-of-flight 3D imaging through multimode optical fibers," Science **374**(6573), 1395–1399 (2021).
15. P. Caramazza, O. Moran, R. Murray-Smith, *et al.*, "Transmission of natural scene images through a multimode fibre," Nat. Commun. **10**(1), 2029 (2019).
16. N. H. Valencia, S. Goel, W. McCutcheon, *et al.*, "Unscrambling entanglement through a complex medium," Nat. Phys. **16**(11), 1112–1116 (2020).
17. R. Fickler, M. Ginoya, and R. W. Boyd, "Custom-tailored spatial mode sorting by controlled random scattering," Phys. Rev. B **95**(16), 161108 (2017).
18. S. Leedumrongwatthanakun, L. Innocenti, H. Defienne, *et al.*, "Programmable linear quantum networks with a multimode fibre," Nat. Photonics **14**(3), 139–142 (2020).
19. S. Yin, P. B. Ruffin, and F. T. S. Yu, eds., *Fiber Optic Sensors* (CRC Press, 2017).
20. K. Grattan and T. Sun, "Fiber optic sensor technology: an overview," Sens. Actuators, A **82**(1-3), 40–61 (2000).
21. X. Liu, B. Jin, Q. Bai, *et al.*, "Distributed Fiber-Optic Sensors for Vibration Detection," Sensors **16**(8), 1164 (2016).
22. S. Kumar, R. Singh, Z. Wang, *et al.*, "(Invited) Advances in 2D nanomaterials-assisted plasmonics optical fiber sensors for biomolecules detection," Results in Optics **10**, 100342 (2023).
23. J. G. V. Teixeira, I. T. Leite, S. Silva, *et al.*, "Advanced fiber-optic acoustic sensors," Photonic Sens. **4**(3), 198–208 (2014).
24. I. Ashry, Y. Mao, A. Trichili, *et al.*, "A Review of Using Few-Mode Fibers for Optical Sensing," IEEE Access **8**, 179592–179605 (2020).
25. X. Bao and Y. Wang, "Recent Advancements in Rayleigh Scattering-Based Distributed Fiber Sensors," Adv. Devices Instrum. **2021**, 8696571 (2021).
26. J. N. Fields and J. H. Cole, "Fiber microbend acoustic sensor," Appl. Opt. **19**(19), 3265_1 (1980).
27. N. J. Lindsey, E. R. Martin, D. S. Dreger, *et al.*, "Fiber–Optic Network Observations of Earthquake Wavefields," Geophys. Res. Lett. **44**(23), 792 (2017).
28. J. A. Bucaro and E. F. Carome, "Single fiber interferometric acoustic sensor," Appl. Opt. **17**(3), 330–331 (1978).
29. M. J. Murray and B. Redding, "Distributed multimode fiber Φ-OTDR sensor using a high-speed camera," OSA Continuum **4**(2), 579 (2021).

Optics EXPRESS


30. T. Nishimoto, T. Miyahara, H. Takehana, *et al.*, "Development of 66 kV XLPE submarine cable using optical fiber as a mechanical-damage-detection-sensor," IEEE Trans. Power Delivery **10**(4), 1711–1717 (1995).
31. R. Di Sante, "Fibre Optic Sensors for Structural Health Monitoring of Aircraft Composite Structures: Recent Advances and Applications," Sensors **15**(8), 18666–18713 (2015).
32. I. García, J. Zubia, G. Durana, *et al.*, "Optical Fiber Sensors for Aircraft Structural Health Monitoring," Sensors **15**(7), 15494–15519 (2015).
33. A. Cutolo, R. Bernini, G. M. Berruti, *et al.*, "Innovative Photonic Sensors for Safety and Security, Part II: Aerospace and Submarine Applications," Sensors **23**(5), 2417 (2023).
34. Y.-J. Rao, "In-fibre Bragg grating sensors," Meas. Sci. Technol. **8**(4), 355–375 (1997).
35. G. M. H. Flockhart, W. N. MacPherson, J. S. Barton, *et al.*, "Two-axis bend measurement with Bragg gratings in multicore optical fiber," Opt. Lett. **28**(6), 387 (2003).
36. X. Chen, C. Zhang, D. J. Webb, *et al.*, "Highly Sensitive Bend Sensor Based on Bragg Grating in Eccentric Core Polymer Fiber," IEEE Photonics Technol. Lett. **22**(11), 850–852 (2010).
37. M. Mazur, D. Wallberg, L. Dallachiesa, *et al.*, "Field Trial of FPGA-Based Real-Time Sensing Transceiver over 524 km of Live Aerial Fiber," in *Optical Fiber Communication Conference (OFC) 2023*, (Optica Publishing Group, Washington, D.C., 2023), p. Tu3G.4.
38. D. Psaltis, D. Brady, X.-G. Gu, *et al.*, "Holography in artificial neural networks," Nature **343**(6256), 325–330 (1990).
39. G. Wetzstein, A. Ozcan, S. Gigan, *et al.*, "Inference in artificial intelligence with deep optics and photonics," Nature **588**(7836), 39–47 (2020).
40. S. Colburn, Y. Chu, E. Shilzerman, *et al.*, "Optical frontend for a convolutional neural network," Appl. Opt. **58**(12), 3179 (2019).
41. F. Léonard, A. S. Backer, E. J. Fuller, *et al.*, "Co-Design of Free-Space Metasurface Optical Neuromorphic Classifiers for High Performance," ACS Photonics **8**(7), 2103–2111 (2021).
42. G. Gibson, J. Courtial, M. J. Padgett, *et al.*, "Free-space information transfer using light beams carrying orbital angular momentum," Opt. Express **12**(22), 5448–5456 (2004).
43. M. P. J. Lavery, G. C. G. Berkhout, J. Courtial, *et al.*, "Measurement of the light orbital angular momentum spectrum using an optical geometric transformation," J. Opt. **13**(6), 064006 (2011).
44. N. K. Fontaine, R. Ryf, H. Chen, *et al.*, "Laguerre-Gaussian mode sorter," Nat. Commun. **10**(1), 1865 (2019).
45. Y. Bengio, A. Courville, and P. Vincent, "Representation Learning: A Review and New Perspectives," IEEE Trans. Pattern Anal. Mach. Intell. **35**(8), 1798–1828 (2013).
46. D. Loterie and D. Psaltis and C. Moser, "Bend translation in multimode fiber imaging," Opt. Express **25**(6), 6263 (2017).
47. N. K. Fontaine, H. Chen, M. Mazur, *et al.*, "Hermite-Gaussian mode multiplexer supporting 1035 modes," *Optical Fiber Communication Conference (OFC) 2021* M3D.4 (2021).
48. T. Doster and A. T. Watnik, "Machine learning approach to OAM beam demultiplexing via convolutional neural networks," Appl. Opt. **56**(12), 3386 (2017).
49. G. C. G. Berkhout, M. P. J. Lavery, J. Courtial, *et al.*, "Efficient Sorting of orbital angular momentum States of Light," Phys. Rev. Lett. **105**(15), 153601 (2010).
50. M. P. J. Lavery, D. J. Robertson, G. C. G. Berkhout, *et al.*, "Refractive elements for the measurement of the orbital angular momentum of a single photon," Opt. Express **20**(3), 2110–2115 (2012).
51. M. P. J. Lavery, "Vortex instability in turbulent free-space propagation," New J. Phys. **20**(4), 043023 (2018).
52. N. Zhao, X. Li, G. Li, *et al.*, "Capacity limits of spatially multiplexed free-space communication," Nat. Photonics **9**(12), 822–826 (2015).
53. S. Lightman, I. Bleyhman, L. Somers, *et al.*, "Integrated orbital angular momentum mode sorters on vortex fibers," Opt. Lett. **47**(14), 3491 (2022).